

Patterns of Wave-orbital Speed and Skin Friction Under Estuarine (Fetch-limited) Waves

T.J. Dolphin[†] and M.O. Green[‡]

[†]School of Environmental Science, University of East Anglia, Norwich, NR47TJ, U.K.
tony.dolphin@uea.ac.uk

[‡]National Institute of Water and Atmospheric Research, P.O. Box 11-115, Hamilton, New Zealand.
m.green@niwa.co.nz



ABSTRACT

DOLPHIN, T.,J. and GREEN, M.O., 2009. Patterns in wave-orbital speed and skin friction under estuarine (fetch-limited) waves. *Journal of Coastal Research*, SI 56 (Proceedings of the 10th International Coastal Symposium), 178 – 182. Lisbon, Portugal, ISSN 0749-0258

Sediment transport on estuarine intertidal flats is complex, due to mixed sediments (muds and sands), wetting and drying, and exposure to spatially and temporally varying tidal currents and the locally generated, fetch-limited, wave field. In comparison to open-coast settings, waves on estuarine flats have received comparatively little attention. In this paper we present the results of field experiments investigating processes that control sediment transport on an intertidal flat in a large New Zealand estuary (fetch lengths up to 25 km) under locally generated waves (wave heights of 0.2 – 1 m and periods of 2 – 6 s). The tidal range is > 4 m on springs and in channels tidal flows can reach 2 m/s. Waves control sediment entrainment as tidal currents are subcritical. During wind events, variation in the near bed wave-orbital speed at any point on the intertidal flat depends on a subtle balance between depth, wave height and period, all of which vary over the tidal cycle. As water level rises, intertidal banks of the central harbour are inundated, fetch increases, and height and period of the fetch-limited waves grow. Whilst increasing depth retards the penetration of wave-orbital motions down to the bed, increasing period and height counteract that, resulting in an increase in wave-orbital speed at the bed, wave-induced skin friction, and sediment entrainment. However, sediment flux may not co-vary with entrainment, since it depends also on the tidal current, which transports the entrained sediment, and which is not necessarily coupled with the wave field. The typical variation over the tidal cycle in the resulting sediment transport is thought to change with elevation on the flat, which has important implications for the morphological zonation on intertidal flats.

ADDITIONAL INDEX WORDS: *intertidal flat, entrainment, sand, silt, penetration*

INTRODUCTION

Sediment transport on estuarine intertidal flats is complex, due to mixed sediment sizes (silts and sands), wetting and drying, and spatially and temporally varying tidal currents and wave-orbital motions under the locally generated, fetch-limited wave field. In comparison to open-coast settings, sediment-transport processes on estuarine flats have received little attention (MALVAREZ, *et al.*, 2001). An accurate understanding of the processes that mobilize and transport sediments on estuarine intertidal flats (and in adjacent channels) is needed to understanding the evolution of estuarine morphology, the burial and dispersal of contaminants, and habitat change, and to developing predictive numerical models. In this paper we present the results of field experiments investigating processes that control sediment transport on an intertidal flat in a large New Zealand estuary (fetch lengths up to 25 km).

SETTING

Manukau Harbour is a large, meso-tidal, barrier-enclosed estuary adjacent to the city of Auckland, New Zealand (Figure 1). The estuary is shallow and infilled, with over 40% of its surface area exposed at low tide. Large intertidal and subtidal flats/banks are dissected by deep tidal-channels. The tide is semi-diurnal with a spring range of 4.4 m. Tidal flows peak around mid-tide (slack water at high and low tide), are strong in deep tidal channels (up to

200 cm/s in the inlet gorge), and weaken with elevation across intertidal flats (0 – 40 cm/s).

The estuary is sheltered from oceanic swells (GORMAN and NEILSON, 1999) by a large Pleistocene barrier (10 x 25 km) and a very large and shallow ebb-tidal delta (1250x10⁶ m³; HICKS and HUME, 1996). Maximum fetch is at high tide (25 km), but on the falling tide intertidal banks (see Figure 1) emerge and the fetch reduces. Optimum conditions for wave generation require coincidence of very strong winds with high spring tides, when fetch is at its maximum. Under such conditions waves can grow to over 1-m high.

Experiments were conducted on the Wiroa intertidal flat, on the eastern side of Manukau Harbour (Figure 1). The site is exposed to prevailing south-westerly winds. The intertidal flat is approximately 2 km wide and has five distinct regions distinguished by variation in slope and sediment size distribution; the channel margin (1:40), lower flat (1:450), middle flat (1:400), upper flat (1:1000) and the estuarine beachface (1:10) (DOLPHIN, 2004). On the channel margins and lower flat, silts make up 3-4% of bed sediments; landward the low gradient sand flat (< 2 % mud) often features wave ripples; on the upper flat low amplitude multiple bars are present (DOLPHIN *et al.*, 1995), sandy sediments give way to mud deposits around discrete patches of mangrove forest; and the upper flat breaks into a steep, shelly coarse-sand beach face.

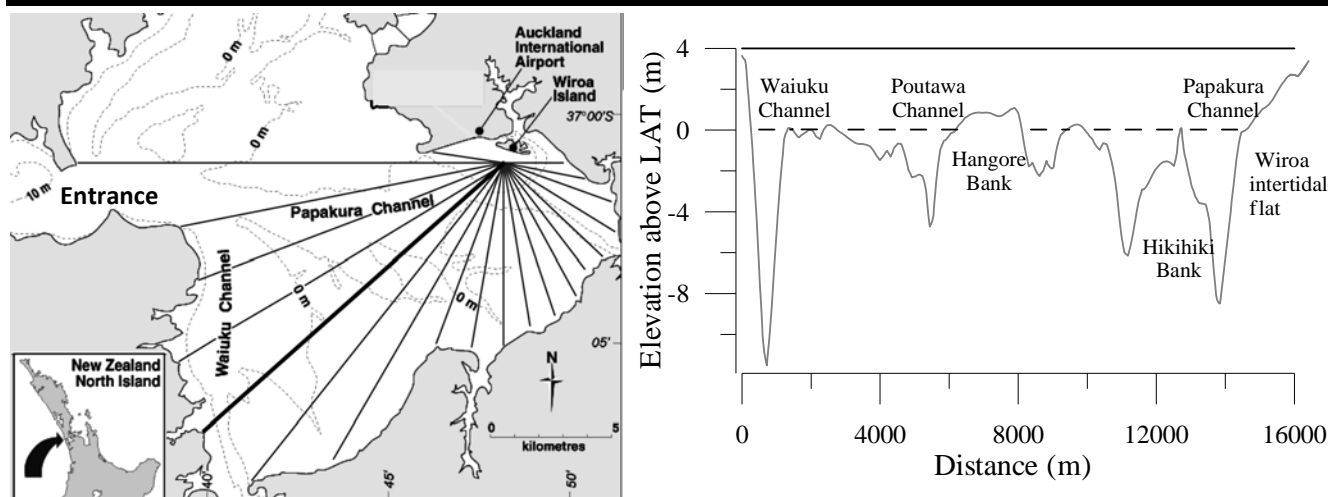


Figure 1: Location map of Manukau Harbour (left panel) and bathymetric profile (right panel) oriented to the prevailing SW wind and leading to the Wiroa intertidal flat (marked by the heavy line on the map).

METHODS

A transect parallel to the prevailing south westerly wind was instrumented at 16 stations. The data used here are from the instrumented tripod, Alice. Alice measures total pressure using a Paroscientific pressure sensor; water currents using four vertically offset Marsh–McBirney 3.8-cm electromagnetic current meters; suspended silt concentration using four vertically offset OBSs; suspended sand concentration using a three frequency (1.08, 1.97 and 4.38 MHz) acoustic backscatter system (ABS); and total suspended sediment concentration and particle size distribution using a purpose built water sampler, Zeldi. Water samples were analyzed in the lab with a Galai time-of-transition particle sizer and using standard filtration techniques for suspended sediment concentration.

The particle-size distribution during storm events is distinctly bi-modal, consisting of silts (10–30 μm) and sands (125–225 μm). Following GREEN *et al.* (1999) and GREEN *et al.* (2000), we used the OBSs to estimate the suspended silt concentration and the ABS to estimate suspended sand concentration. The OBSs are comparatively insensitive to sand in suspension - assuming only silt is present in a 1:1 silt:sand mixture gives a 10% error. The ABS is comparatively insensitive to silt in suspension - assuming only sand is present in a 1:1 silt:sand mixture gives a 0.5% error.

Estimates of the skin friction under waves and currents were determined from current meter data as follows. For steady currents, the skin friction is:

$$u'_{*c} = \kappa \bar{U}(z) / \ln(z/z'_0) \quad (1)$$

where $z'_0 = 2.5d_s/30$ is the skin-friction roughness length, d_s is the particle diameter, \bar{U} is the steady current at elevation z , and κ is von Karman's constant (0.41). The friction velocity u'_{*c} can be nondimensionalised by:

$$\theta'_c = \frac{\rho_f u'^2_{*c}}{(\rho_s - \rho_f)gd_s} \quad (2)$$

which can then be used to estimate entrainment by comparing θ'_c with the critical Shields parameter for initiation of sediment

motion, θ'_{cr} (see Entrainment section). For evaluating equations 1 and 2, d_s was taken as 180 μm for sand and 20 μm for silt, and \bar{U} was determined from current measurements made at the nominal elevation $z = 13.5$ cm.

Under waves, the skin-friction friction velocity is estimated as:

$$u'_{*w} = U_w \sqrt{0.5f'_w} \quad (3)$$

where U_w is the wave-orbital speed at the bed and f'_w is the skin-friction wave friction factor, evaluated as $f'_w = \exp[5.213(2.5d_s/a_w)^{0.194} - 5.977]$ (SWART, 1974), where a_w , the wave-orbital radius, is related to the wave-orbital speed as $U_w = a_w\omega$, and ω is the wave radian frequency. u'_{*w} can be nondimensionalised as shown in equation 2 to give the dimensionless wave-induced skin friction θ'_w . Following BLACK and ROSENBERG's (1991) work on velocity scales and sediment transport, the 3rd orbital-speed moment (U_3) was chosen to represent U_w in the evaluation of equation 3. The nondependence of U_3 on Rayleigh wave statistics (e.g., U_{rms} , U_s) also serves to free the skin-friction calculations from assumptions relating to Rayleigh distributed sea-surface elevations.

RESULTS

Entrainment

The relative abilities of steady currents and waves to entrain of bed sediment are assessed in Figure 2 where, for each burst, θ'_w is plotted against θ'_c . For each burst entrainment is defined according to whether sediment was observed to be in suspension or not. The resulting 'suspension' and 'no-suspension' categories are shown as filled and hollow symbols in Figure 2.

Sand entrainment on the Wiroa intertidal flat is dominated by waves, as shown by the near-horizontal separation of filled (suspension) and hollow (no-suspension) symbols in Figure 2 (left panel). The entrainment threshold inferred from the data (0.05), is very similar to the value predicted (0.056) using the Shields curve proposed by SOULSBY and WHITEHOUSE, (1997):

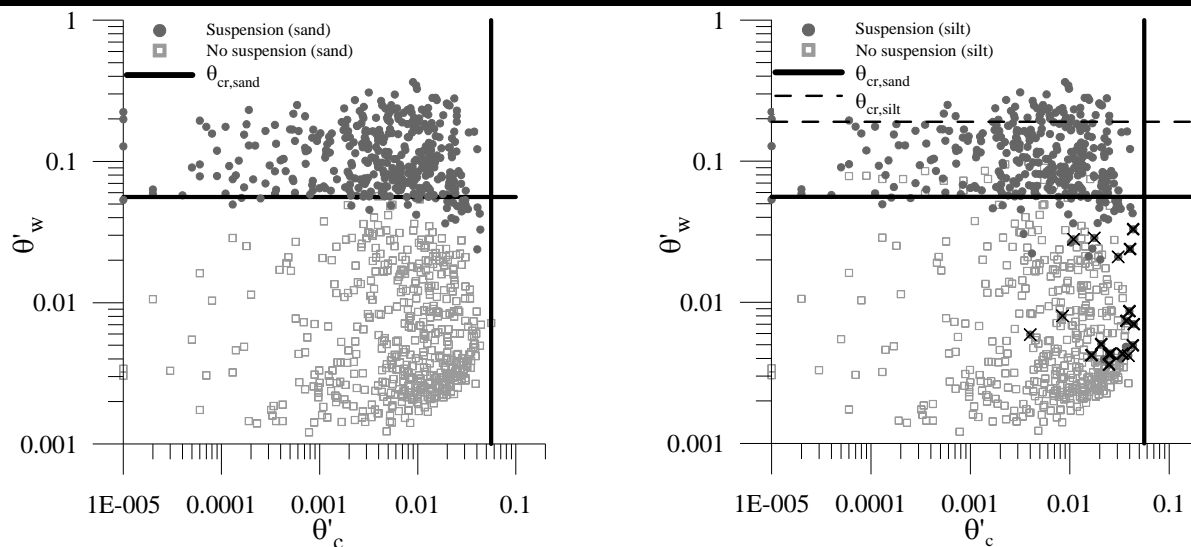


Figure 2: Skin friction due to waves (θ'_w) versus skin friction due to currents (θ'_c). Data are classified according to whether sand (left panel) or silt (right panel) is in suspension (filled symbols) or not (hollow symbols) indicate “no suspension”. The solid line is the predicted sand entrainment threshold $\theta_{cr,sand}$, and the dashed line is the predicted silt entrainment threshold $\theta_{cr,silt}$ (equation 5).

$$\theta_{cr} = \frac{0.24}{D^*} + 0.055[1 - \exp(-0.020D^*)] \quad (5)$$

where D^* is the dimensionless grain size

$$D^* = \left[\frac{g(s-1)}{\nu^2} \right]^{1/3} d_s, \quad (6)$$

s is the ratio of sediment and water densities, ν is the kinematic viscosity, and g is acceleration due to gravity. Figure 2 also shows that currents alone were never capable of entraining sand, which is also consistent with the predicted critical Shields parameter. Therefore, equation 5 is a good predictor of sand entrainment on the Wiroa intertidal flat under both pure waves and pure currents.

Silt entrainment on the Wiroa intertidal flat is also dominated by waves, as shown by the near-horizontal separation of filled (suspension) and hollow (no suspension) symbols in the right panel of Figure 2. Compared to sand, however, the dividing line between suspension and no suspension is less distinct, which indicates that waves alone are not as good a predictor of silt entrainment. Another factor that may affect suspended-silt concentration on intertidal flats is rainfall, which delivers runoff laden with fine sediments to the wider harbour. This seems to be the case here, as most the “outlier bursts” (bursts for which silt was in suspension but neither θ'_c nor θ'_w exceeded the theoretical value of $\theta_{cr,silt}$) did correspond to times of heavy rainfall (bursts marked with an “X” in Figure 2). A further explanation could be that silt observed in suspension at the measurement site was actually entrained from the bed at a more distant site, and carried in suspension to the Wiroa flat. This is less likely to happen with sand, since sand has a larger setting speed compared to silt.

Wave modulation

Wind-waves are strongly modulated by the effect that tidal stage and shallow bathymetry have on fetch length (Figure 3). At low tide, intertidal banks are exposed and fetch is restricted to the 2-km width of the Papakura Channel (see Figure 1). As the tide rises the banks of the central harbour are submerged and fetch increases until high tide. The opposite occurs on the falling tide. As a result, fetch length varies on a 12.4-h cycle, in phase with the tidally varying water level.

The wave height and period measured on the intertidal flat also evolve through the tidal cycle as a result of tidally varying fetch length (Figure 3). Notwithstanding changes in the wind speed and direction, the significant wave height H_s is largest around high tide, when fetch is greatest, and smallest around low tide, when fetch is restricted to the channel width. Wave period (T) evolves in a similar way, but with the peak period in each tidal cycle occurring about two hours after high tide, but whilst fetch is still at a maximum. This resulting asymmetric pattern in the T time-series reflects the ‘storm’ duration at maximum fetch – that is, the longest (and often highest) waves occur toward the end of the high-tide fetch period. The sudden reduction in fetch from 16 – 7 km as the Hangore Bank emerges results in rapid decline in H_s and T .

Relative water depth (kh) and wave-orbital speed

The change in relative water depth $kh = 2\pi h/L$ (where L is wavelength and h is water depth) over the tidal cycle (Figure 3) is driven by the tidal change in water depth as well as changes in the wavelength, which are related to changes in fetch, as previously described. Two observations are noteworthy. Firstly, the decrease in kh on the falling tide is slower than the increase in kh on the rising tide. The rate of change in h is about the same on both sides of the tide, indicating that there is a hysteresis or lag in the decay of L on the falling tide. Secondly, kh is maximum at high tide, and so the relative penetration of wave-orbital motions down the bed will correspondingly be minimum at high tide (Figure 4).

In addition to the influence of the relative water depth kh , changes in the intrinsic wave period over the tidal cycle (1 – 4 s) will also exert a strong control on penetration ($\chi = 1/\sinh[kh]$) and therefore near bed wave-orbital speed ($U_{s,bed} = \chi H_s \pi / T$) at Wiroa. Under a more-or-less constant wind speed, increasing h (and therefore fetch) typically leads to increasing H_s , but decreasing χ . As a result, temporal patterns in $U_{s,bed}$ are determined by a balance between h , H_s and T , all of which increase and decrease over the tidal cycle (Figure 3). On the rising tide, the effect of increasing depth on χ (Figure 4) is countered by the effect of increasing wave period on χ , whilst increasing H_s also acts to increase $U_{s,bed}$. In the first case of Figure 4, $U_{s,bed}$ is in phase with χ^* and kh , but 180° out of phase with H_s . That is, the smaller waves near the beginning

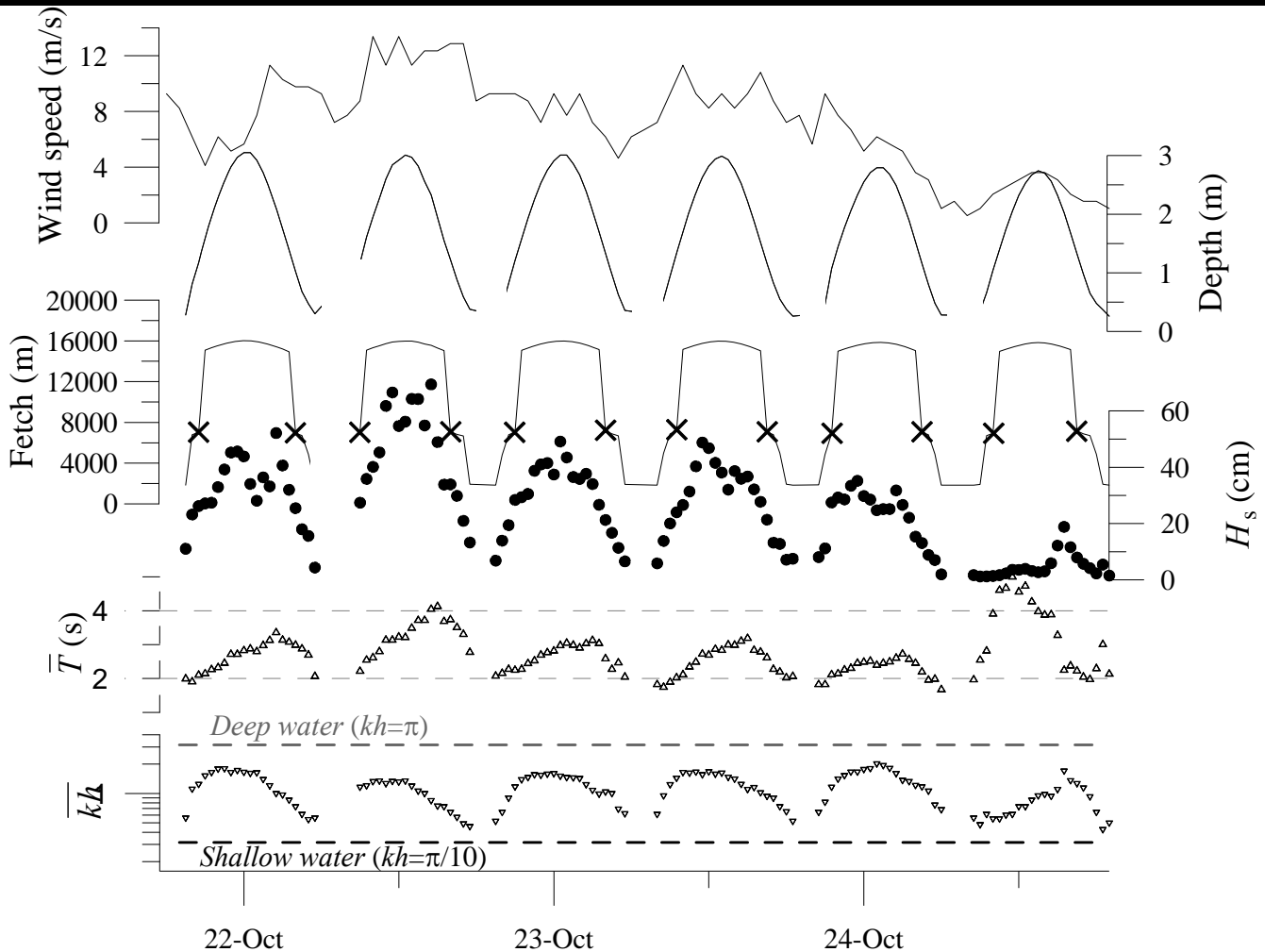


Figure 3: Time-series of wind speed and fetch length with wave and water-depth statistics measured on the Wiroa intertidal flat.

and end of the tidal inundation produce the largest $U_{s,bed}$ when the water is shallow, whilst the largest waves produce smallest $U_{s,bed}$ due to small χ^* . The second case of Figure 4 applies to neap tides and higher elevations on the flat where the high-tide depth is less. In this case χ^* is larger, indicating greater penetration, and despite the lowest χ^* occurring at high tide, increasing wave height dominates the $U_{s,bed}$ signal such that it is in phase with H_s and 180° out of phase with χ^* .

DISCUSSION AND CONCLUSIONS

Despite its mesotidal setting, sand entrainment on the Wiroa intertidal flat at the Alice site is controlled solely by waves. Silt entrainment is similarly controlled by waves, which may be due to the arrangement of silts and sands in the mixed-size bed. Over most of the flat, silts occupy $< 2\%$ of the surficial sediments and do not overlie sands. Instead they probably reside within the interstitial spaces between sand grains and are consequently shielded from overlying bed shear stresses until they are exposed when sand grains begin to move.

In shallow infilled estuaries, fetch (and therefore wave height) is a function of tidal stage, the size and shape of the estuary and the direction from which the wind blows. Large waves can be generated in elongate lagoons and fjords, for example, if the prevailing winds coincide with the long fetch axis, or comparatively small waves if not (e.g., Strangford Lough, RYAN

and COOPER, 1998; MALVAREZ *et al.*, 2001). In Manukau Harbour, the squarish geometry is favorable for large fetches under every wind direction. At Wiroa Island, the largest waves coincide with high-tide fetches (14–18 km) and winds from the prevailing SW sector.

Sediment transport on estuarine intertidal flats, such as Wiroa, is likely to be controlled by the timing of wave-induced entrainment events with respect to the strength of the mean (tidal) current. For example, in the second case shown in Figure 4, $U_{s,bed}$ is largest at high tide, which at the Alice site coincides with high slack water and a low mean current (DOLPHIN, 2004). The resultant sediment flux integrated over the tidal cycle is expected to be smaller than for the first case, where large $U_{s,bed}$ coincides with higher mean currents close to the beginning and end of the inundation. Thus the timing of peak tidal flows relative to water level, which controls penetration as well as fetch and wave growth, will determine sediment flux for each tidal cycle.

An additional factor is the cross-shore spatial variation in both $U_{s,bed}$ and the mean current. Figure 4 suggests that higher elevations on the intertidal flat are more likely to experience a case 2 $U_{s,bed}$ pattern (in phase with H_s), due to lower h and larger χ . If slack water coincides with high tide, then the sediment flux will be lower than if peak current occurs at high tide. Transport potential is also expected to decline with distance up the intertidal flat due to weaker tidal flows at higher elevations (ALLEN, 1971; DYER, 1989). For these ideas to be tested, measurements of waves,

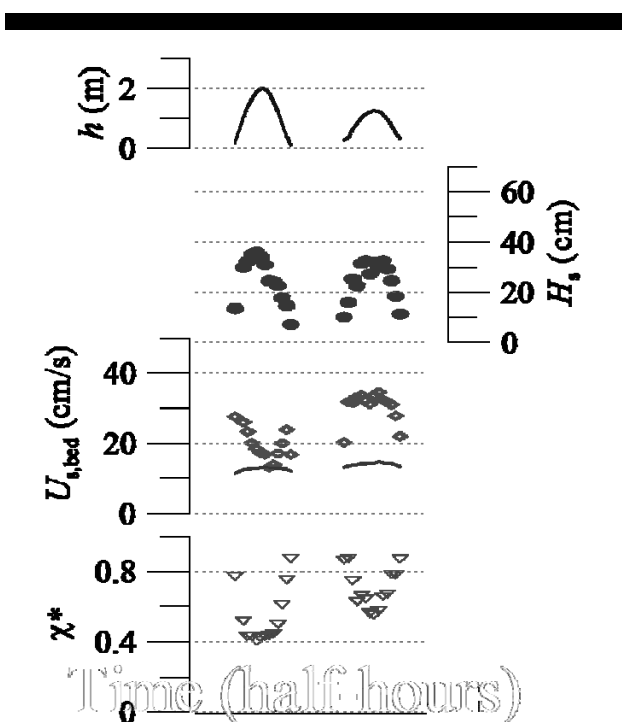


Figure 4. Examples of χ^* ($1/\cosh(kh)$) and $U_{s,bed}$ for two selected tidal cycles. χ^* is plotted instead of χ to describe penetration of the wave signal as it is easier to interpret, nondimensional and scales as a proportion of the surface wave fluctuation. The black line is the Komar and Miller (1975) entrainment threshold. The interval between data points is 30 minutes.

currents and sediment suspension are required across the width of intertidal flats.

To summarize, in large infilled estuaries like Manukau, the periodic emergence and submergence of central intertidal banks will modulate wave parameters that can control entrainment on fringing intertidal flats. These results and others (e.g., GREEN *et al.*, 1999 and GREEN *et al.*, 2000) suggest that waves in large infilled estuaries are an important driver of sediment transport and are likely to play some part in the evolution of intertidal flat morphology.

LITERATURE CITED

- ALLEN, G.P., 1971. Relationship between grain size parameter and current patterns in the Gironde estuary, *Journal of Sedimentary Petrology*, 42 (3), 74-88.
- BLACK, K.P. and ROSENBERG, M.A., 1991. Suspended load at three time scales. In: KRAUS, C.N., GINGERICH, K.J. and MCDUGAL, G.W. (eds), *Coastal Sediments '99*, 1: 644-658.
- DOLPHIN, T.J., HUME, T.M., and PARNELL, K.E., 1995. Oceanographic processes and sediment mixing on a sand flat

in an enclosed sea, Manukau Harbour, New Zealand, *Marine Geology*, 128: 169-181.

- DOLPHIN, T.J., 2004. Wave-induced sediment transport on an estuarine intertidal flat. Hamilton, New Zealand: University of Waikato, Ph.D. thesis, 154 p.
- DYER, K.R., 1989. Sediment processes in estuaries: Future research requirements, *Journal of Geophysical Research*, 94(C10): 14327-14339.
- GORMAN, R.M. and NEILSON, C.G., 1999. Modelling shallow water wave generation and transformation in an intertidal estuary. *Coastal Engineering*, 36: 197-217.
- GREEN, M.O., DOLPHIN, T.J., SWALES, A., and VINCENT, C.E., 1999. Transport of mixed-sediments in a tidal channel. In: KRAUS, C.N. and MCDUGAL, G.W. (eds), *Coastal Sediments '99*, 1, 644-658.
- GREEN, M.O., ROBERT G. BELL, DOLPHIN, T.J., and SWALES, A., 2000. Silt and sand transport in a deep tidal channel of a large estuary (Manukau Harbour, New Zealand), *Marine Geology*, 163, 217-240.
- HICKS, D.M. and HUME, T.M., 1996. Morphology and size of ebb tidal deltas at natural inlets on open-sea and pocket-bay coasts, North Island, New Zealand, *Journal of Coastal Research*, 12(1): 47-63.
- KOMAR, P.D. and MILLER, M.C., 1975. On the comparison between the threshold of sediment motion under waves and unidirectional currents with a discussion of the practical evaluation of the threshold. *Journal of Sedimentary Petrology*, 45: 362-367.
- MALVAREZ, G.C., COOPER, J.A.G., JACKSON, D.W.T., and NAVAS, F., 2001. The role of wave action on sedimentation of tidal flats: Application of high spatial resolution numerical modelling in Strangford Lough, Northern Ireland, *Journal of Coastal Research*, Special Issue 34: 172-182.
- RYAN, N.M. and COOPER, J.A.G., 1998. Spatial variability of tidal flats in response to wave exposure: examples from Strangford Lough, Co. Down, Northern Ireland. In: BLACK, K.S., PATERSON, D.M. and CRAMP, A. (Editors), *Sedimentary Processes in the Intertidal Zone*. Geological Society Special Publications, The Geological Society, London, pp. 221-230.
- SWART, D.H., 1974. *Offshore sediment transport and equilibrium beach profiles*. Delft Hydraulics Lab. Publ. 131.
- SOULSBY, R.L. and WHITEHOUSE, R.J.S., 1997. Threshold of sediment motion in coastal environments. *Proceedings of: Pacific Coasts and Ports: The 13th Australasian Coastal and Ocean Engineering Conference* (Centre for Advanced Engineering, Christchurch, New Zealand), 1: 149-154.

ACKNOWLEDGEMENTS

We would like to acknowledge the Waves in Fluids Group, Centre for Nonlinear Studies, Institute of Cybernetics, Tallinn University of Technology (Estonia), for constructive comments during TD's visiting researcher placement, which was funded by TK project CENS-CMA, MC-TK-013909. We would also like to acknowledge the field assistance of Ian Blair and comments on earlier work by Phil Osborne and Gonzalo Malvarez.